Palaeogeography, Palaeoclimatology, Palaeoecology 561 (2021) 110069

Contents lists available at ScienceDirect

Palaeogeography, Palaeoclimatology, Palaeoecology

journal homepage: www.elsevier.com/locate/palaeo

Climate-driven connectivity changes of the Black Sea since 430 ka: Testing a dual palynological and geochemical approach

Thomas M. Hoyle[a,1], Diksha Bista[b,2], Rachel Flecker[b], Wout Krijgsman[a], Francesca Sangiorgi[a,*]

[a] Department of Earth Sciences, Utrecht University, Vening Meineszgebouw A, Princetonlaan 8a, 3584 CB Utrecht, the Netherlands
[b] BRIDGE, School of Geographical Sciences and Cabot Institute, University of Bristol, University Road, Bristol BS8 1SS, UK

ARTICLE INFO

Keywords:
Dinoflagellate cysts
Strontium isotopes
Pontocaspian region
Late Quaternary
Connectivity

ABSTRACT

The Black Sea experienced multiple episodes of connection with both the Mediterranean and Caspian seas during the Quaternary. Global sea-level variation has been proposed as the main driver of changes in Mediterranean-Black Sea connectivity, while positive water budgets drove Caspian overspill. We present a new, two proxy, low-resolution record from the Black Sea that allows reconstruction of connectivity history from 430 to 50 ka: dinoflagellate cysts (dinocysts) provide direct evidence for properties of surface waters and strontium isotopes constrain the source(s) of water entering the basin. Dinocysts and $^{87}Sr/^{86}Sr$ suggest that the Black Sea was isolated from the Mediterranean during global sea-level lowstands associated with glacials MIS 4, 8 and 10. Both proxies also strongly suggest that marine (Mediterranean) water flowed into the Black Sea during the eustatic highstands associated with peak interglacials during MIS 5 and 9. However, while the contribution of marine waters during MIS 5e was similar to the present day, lower $^{87}Sr/^{86}Sr$ during MIS 9 suggests lower than present input. Connectivity during MIS 11, MIS 7 and MIS 6 is more enigmatic. Lower $^{87}Sr/^{86}Sr$ than those of the isolated Black Sea and dinocyst assemblages dominated by species of Paratethyan lineage are compatible with input from the Caspian Sea. Dinocyst taxa recovered in MIS 11 can be found in both the Caspian Sea and the Black Sea today. All four interglacials studied contain different dinocyst assemblages, suggesting that different conditions may have prevailed during each warm period. However, high-resolution studies are needed to confirm this observation. Further work on the same sequence could be valuable in elucidating the connectivity history of the Black Sea over the glacial-interglacial cycles of the late Quaternary.

1. Introduction

At present, the Black Sea is connected to the global ocean via the Marmara Sea, Aegean and Mediterranean. However, the Black Sea has previously been isolated from the Mediterranean Sea for significant periods (e.g. Krijgsman et al., 2020; Schrader, 1978). Change in sea-level due to glacial-interglacial cycles has been suggested as the main driver of Quaternary Mediterranean-Black Sea connectivity, with connections occurring during interglacial sea-level highstands (Schrader, 1978). In addition, mollusc records from the Caspian and Black Sea basins suggest that the Caspian Sea spilled into the Black Sea on several occasions during the late Quaternary (Svitoch et al., 2000; Yanina et al., 2017; Zubakov, 1988). Biostratigraphic correlation between the Caspian Sea and Black Sea basins is difficult, especially prior to the last interglacial, Marine Isotope Stage (MIS) 5e, ~125 thousand years before present (ka), as it is commonly based on the spatial occurrence of endemic faunas, and absolute age determinations are rare (Krijgsman et al., 2019). Well-dated negative oxygen isotope excursions in speleothem from Sofular cave in Turkey during MIS 7 (220 ka) and MIS 6 (175 ka) (Badertscher et al., 2011) have also been interpreted as indicating Caspian input to the Black Sea at these times. Depleted speleothem calcite $\delta^{18}O$ values were attributed to isotopically depleted precipitation over Anatolia derived from a fresh water surface layer in the Black Sea caused by overspill from the Caspian (Badertscher et al., 2011). However, although faunal data indicate the occasional incursion of characteristic Caspian Sea molluscs into the Azov region (Yanina, 2012) there is no explicit evidence of Caspian over-spill during MIS 7 and 6 from published records in the deep basin areas of the Black Sea (Krijgsman et al., 2019).

* Corresponding author.
E-mail addresses: thomas.hoyle@casp.org.uk (T.M. Hoyle), diksha.bista@bristol.ac.uk (D. Bista), R.Flecker@bristol.ac.uk (R. Flecker), W.Krijgsman@uu.nl (W. Krijgsman), f.sangiorgi@uu.nl (F. Sangiorgi).
[1] Now at: CASP, West Building, Madingley Rise, Madingley Road, Cambridge CB3 0UD, UK.
[2] Now at: NERC Isotope Geosciences Laboratory, British Geological Survey, Keyworth NG12 5GG, UK.

https://doi.org/10.1016/j.palaeo.2020.110069
Received 12 June 2020; Received in revised form 24 September 2020; Accepted 24 September 2020
Available online 02 October 2020

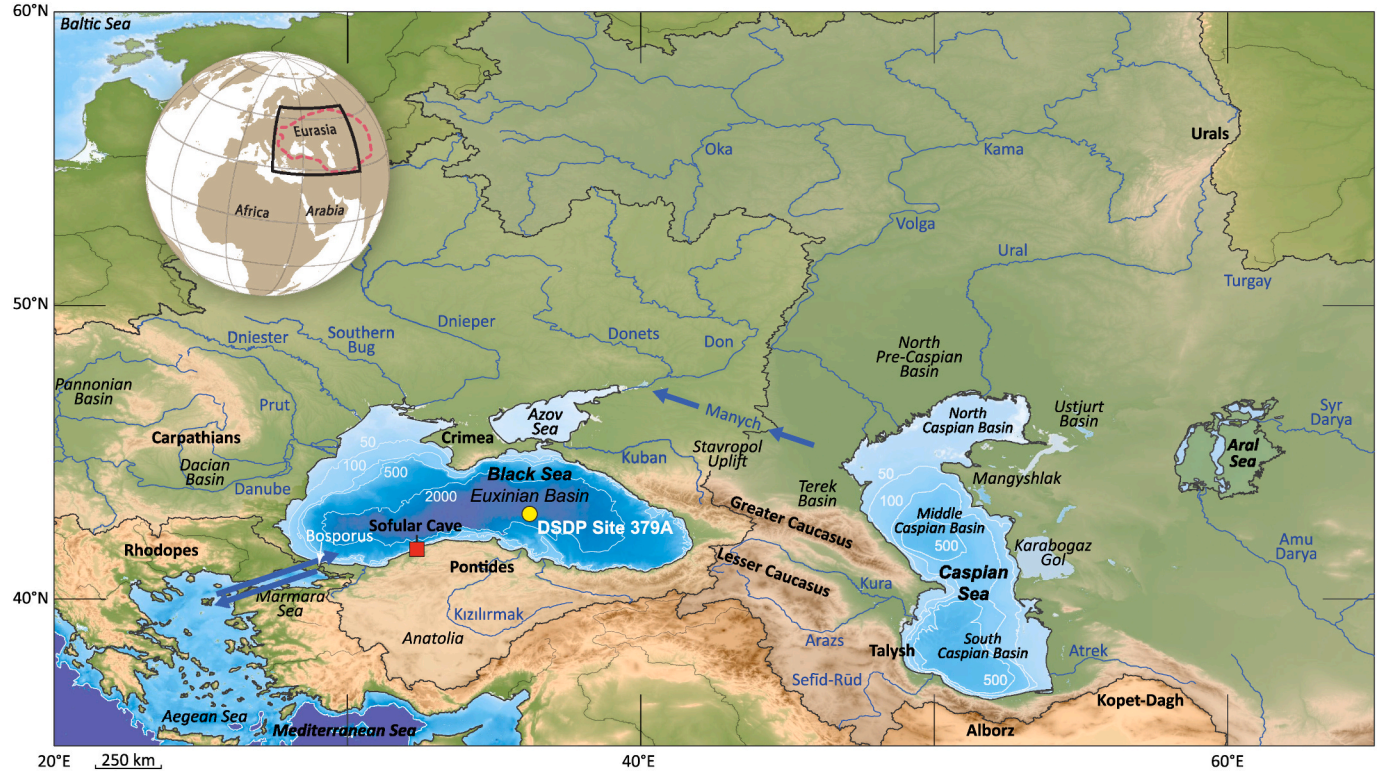

Fig. 1. Map of the study area showing the Black Sea and Caspian Sea region. Yellow dot indicates location of Deep Sea Drilling Project (DSDP) Site 379 (43°00.29′N; 36°00.68′E). Red square indicates the location of Sofular Cave. Locations of the Manych spillway, Bosporus strait and all major rivers are indicated. Figure modified after Krijgsman et al. (2019). (For interpretation of the references to colour in this figure legend, the reader is referred to the web version of this article.)

Here, by testing a new dual proxy approach, we aim to provide a preliminary (low-resolution) reconstruction of the connectivity history of the Black Sea with the Mediterranean Sea and the Caspian Sea during the late Quaternary (MIS 11 to 4) using dinoflagellate cysts (dinocysts) as tracers of surface water properties and strontium isotope ratios on ostracod valves as tracers of water input source(s). Both proxies are determined on the same sample. We also use variations in the amount and composition of climate-related pollen species from terrestrial plants to constrain correlation to glacial-interglacial fluctuations. Ideally, each interglacial will show a fingerprinting combination of assemblage studies and strontium isotopes that may be of stratigraphic importance.

2. Materials and methods

2.1. Sediments

The nineteen samples considered in this study were taken from the upper ~275 m (45.54 to 272.13 m below sea floor, mbsf) of the Deep Sea Drilling Project (DSDP) Site 379 record (Fig. 1), which was drilled in the central part of the Black Sea (43°00.29′N; 36°00.68′E, 624.5 m water depth) in May 1975 (Shipboard Scientific Staff, 1978). Cores were sub-sampled at the International Ocean Discovery Programme (IODP) core repository in Bremen, Germany (see supplementary information for core information and sample depths). Samples were chosen to potentially capture the strongest climate shifts in the late Quaternary. According to the age model of Van Baak et al. (2016) these samples span the interval 430–50 ka.

2.2. Palynological processing

Samples were processed using cold HCl (30%) to remove carbonates and cold HF (38%) to dissolve silicates. Samples were subjected to five minutes in an ultrasonic bath and sieved through 125 and 10 μm meshes. The 10–125 μm fraction was retained and mounted on slides using glycerine jelly and sealed with lacquer. Counting was carried out at magnifications of × 400 and × 1000 using a binocular transmitted light microscope.

Dinocyst identifications were made using plates and descriptions in various reference texts (Marret et al., 2004; Mudie et al., 2004; Mudie et al., 2001; Rochon et al., 2002; Rochon et al., 1999; Shumilovskikh et al., 2013b; Sütő-Szentai, 2010; Wall et al., 1973; Wall and Dale, 1973) and taxa that fell along morphological gradients were grouped/split according to the dinocyst variability matrix of Hoyle et al. (2019). Pollen identifications were made using plates and descriptions in Menke (1976), Moore and Webb (1978) and Reille (1992). A known number of *Lycopodium clavatum* spores was added to each sample prior to processing in order to monitor concentrations.

Palynological data were processed using Psimpoll 4.27 (Bennett, 2008). Dinocyst data are represented as a percentage of the dinocyst sum (average for this study = 220), which included all identified dinocysts (possessing an archeopyle) but excluded acritarchs, foraminiferal test linings, unidentified cysts and any other algal or aquatic taxa. Additional non-dinocyst aquatic palynomorphs are represented in the diagram as a percentage of the total aquatic palynomorph count. Pollen data are shown as a percentage of the terrestrial pollen sum (average for this study = 335), which includes pollen of terrestrial gymnosperms and angiosperms only. Other terrestrially derived non-pollen palynomorphs, such as spores and fungal material, were counted in addition to the pollen sum.

2.3. Palynology for environmental reconstructions

Dinoflagellate cysts (dinocysts) respond to sea surface water conditions (e.g., Zonneveld et al., 2013; Marret et al., 2020; Mudie et al., 2017). As such, where their ecological affinities are known, they can be used as proxies to reconstruct palaeoenvironments with a high degree

of accuracy (e.g., De Vernal and Marret, 2007). Dinocyst paleoenvironmental studies of Black Sea sediments have mainly focussed on the late glacial to Holocene (Mertens et al., 2009; Mudie et al., 2007; Mudie et al., 2004; Mudie et al., 2001) and to a lesser extent, the last interglacial period (Ferguson et al., 2018; Shumilovskikh et al., 2013b).

An extraordinary array of inter- and intraspecific variability is observed in dinocysts from the the Pontocaspian (Black Sea, Caspian Sea and Aral Sea) basins, which display greater variability than in open ocean settings (Marret et al., 2004; Mudie et al., 2001; Wall et al., 1973; Wall and Dale, 1973; Hoyle et al., 2019). However, even though the taxonomy of these dinocysts is complex, certain key forms and ecophenotypic traits are strong indicators of cyst production under different environmental conditions. Cruciform shape and dorso-ventral compression, reduced processes and the development of apical nodes, for example, have been noted as features characteristic of dinocysts living in lower than marine salinities (Mertens et al., 2009; Mudie et al., 2017; Hoyle et al., 2019). Several characteristic endemic forms have also been present in the region since the Miocene, and can be used to provide further palaeoenvironmental constraints, in particular as indicators of low salinities (oligohaline to lower mesohaline) (Rundić et al., 2011; Soliman and Riding, 2017).

Dinocysts have been here used for salinity estimates based on information derived from a combination of culture studies (Ellegaard et al., 2002; Lewis et al., 2018), and studies relating surface sediment cyst assemblages with modern sea surface conditions (Mudie et al., 2017; Zonneveld et al., 2013). In cases where no living analogue is known, estimates of contemporary sea surface conditions are inferred from the geological setting and associated fossils (Baltes, 1971; Cziczer et al., 2009; Kouli et al., 2001; Leroy and Albay, 2010; Soliman and Riding, 2017).

Pollen were grouped according to their environmental affinities. Here, the deciduous forest category includes *Betula*, *Fraxinus*, *Engelhardia*, *Juglans*, *Carya*, *Pterocarya*, *Acer*, *Tilia*, *Ulmus-Zelkova*, *Carpinus*, *Quercus*, *Alnus*, *Fagus*, *Castanea*, *Nyssa*, *Salix*, *Myrica* and *Corylus*. Altitudinal conifer forest includes *Abies*, *Picea*, *Tsuga* and *Cedrus*. The xerophytic category includes *Ephedra*, Amaranthaceae, Caryophyllaceae, Asteraceae (including *Artemisia* and *Centaurea*), Convolvulaceae, Poaceae, *Calligonum* and *Rhus*.

2.4. Processing for strontium isotopes

Sediment samples (~100 g) were washed and sieved at 60 μm then dried at 50 °C. Samples were dry sieved to retain the > 150 μm fraction and 2–5 smooth, clean ostracod valves were picked under a stereomicroscope. Where ostracod valves were sufficiently abundant, Sr isotope analysis was carried out on whole valves. However, in the majority of samples, ostracod remains were relatively rare and a few fragments were used instead. In some samples it was not possible to perform both dinocyst counting and Sr isotope analysis because of there being either no ostracods or no dinocysts preserved. Where possible both analyses were performed on the same samples.

The ostracods were collected in an acid cleaned, pre-labelled vial and rinsed three times using MilliQ water. Samples were subjected to 5 s in an ultrasonic bath after every rinse to remove any loose clay particles. Samples were then cleaned twice with methanol to remove organics and rinsed again twice with MilliQ water to remove traces of methanol.

Samples were dissolved using 300 μl of 0.1 M HNO_3 and 2 min in an ultrasonic bath. They were then centrifuged for 3 min at 12,000 rpm to separate any residue and the solution was carefully transferred into acid cleaned Teflon beakers and dried at 120 °C on a hot plate.

A few drops of concentrated HNO_3 were added to the samples to remove organics and dried at 120 °C. Once dried, the samples were refluxed using 500 ml of 3 M HNO_3 on the hot plate at 120 °C. Sr was then extracted from the samples by introducing them to chromatographic columns composed of “Eichrom Sr Resin”.

Each sample was then loaded onto a single tungsten filament with $TaCl_2$ as an activator (Birck, 1986). The strontium isotopic analysis was carried out at the Bristol Isotope Group facilities in University of Bristol. The $^{87}Sr/^{86}Sr$ was measured using multi dynamic method in a Thermo Scientific™ Triton thermal ionization mass spectrometer (TIMS). Instrument performance was monitored using NBS 987 Sr standard, which produced average 0.710249 ± 0.000009 (2 SD, n = 15) over the course of the study. The procedural blank is considered negligible, based on replicate measurement of NBS 987 standards with each batch of chemical processing and column chromatography. These standards give an average value of 0.710247 ± 0.000005 (n = 8).

2.5. Strontium isotopes interpretations

The strontium isotope ratio ($^{87}Sr/^{86}Sr$) of any water body is dependent on the $^{87}Sr/^{86}Sr$, strontium concentration and volume of all its inputs. In lacustrine settings, the $^{87}Sr/^{86}Sr$ is controlled by the catchment geology of the rivers supplying water and sediment to the basin, with different signals resulting from catchments draining different rock types (Palmer and Edmond, 1989). The average concentration of strontium in rivers (0.2–0.5 ppm) is significantly lower than that of ocean water (~8 ppm) (Palmer and Edmond, 1989; Veizer, 1989). Consequently, even a relatively small input of oceanic water to a lacustrine basin can overprint the riverine signal. It is for this reason that the present-day Black Sea Sr isotope ratio is within error of today's ocean water value (Major et al., 2006; McArthur et al., 2012).

The $^{87}Sr/^{86}Sr$ of water is incorporated into biogenic carbonate without measurable fractionation (Reinhardt et al., 1999). This primary isotopic record can then be used to reconstruct past $^{87}Sr/^{86}Sr$ of the water body (e.g. Burke et al., 1982; Henderson et al., 1994; McArthur et al., 2012). In non-marine settings, ostracod valves are an excellent Sr isotope archive because they are relatively abundant and their low Mg-calcitic composition is not prone to diagenetic alteration (Bennett et al., 2011; Brand and Veizer, 1980). The $^{87}Sr/^{86}Sr$ record of a basin can then be interpreted using river and ocean values of $^{87}Sr/^{86}Sr$ and Sr concentration of likely contributing water sources. This makes strontium isotope ratios an excellent method for reconstructing connectivity both between marginal or lacustrine basins and with the open ocean (Albarède and Michard, 1987; Ingram and Sloan, 1992; Reinhardt et al., 1998). Strontium isotopes have been used in this way to reconstruct the evolution of Black Sea composition over the last deglaciation, as well as in the Mio-Pliocene of the Paratethyan basins (e.g., Major et al., 2006; Vasiliev et al., 2010; Grothe et al., 2020).

2.6. Steady-state strontium values

The basin connectivity status of the Black Sea can fit into any of four steady state scenarios. The Black Sea can be: a) in its present day configuration, experiencing two-way exchange with the Mediterranean Sea (Fig. 2 **a**); b) in the same state as during Last Glacial Maximum, isolated from all adjacent basins **(**Fig. 2 **b);** c) receiving input only from the Caspian Sea (Fig. 2 **c);** or d) receiving input from both the Caspian Sea and the Mediterranean Sea (Fig. 2 **d**). Measured Sr isotope ratios from Major et al. (2006) are presented for the potential contributing sources as well as for the Black Sea in the present day (with the Black Sea connected to the Mediterranean) and the Last Glacial Maximum (with the Black Sea isolated from the Mediterranean) (Table 1). These values were compared with theoretical values produced using a mass balance calculation (eq. 3), which produced a marginally higher value for the present-day and value within error for the Last Glacial Maximum. Such a minor discrepancy between the observed and calculated values for the present-day Black Sea may be attributed to the influence of small rivers not considered in eq. 3. Additional data would be needed to further constrain the impact of Sr data for the minor rivers draining the coast of Turkey, Bulgaria and Georgia. However, the magnitude of their combined discharge is so small compared to that of the three

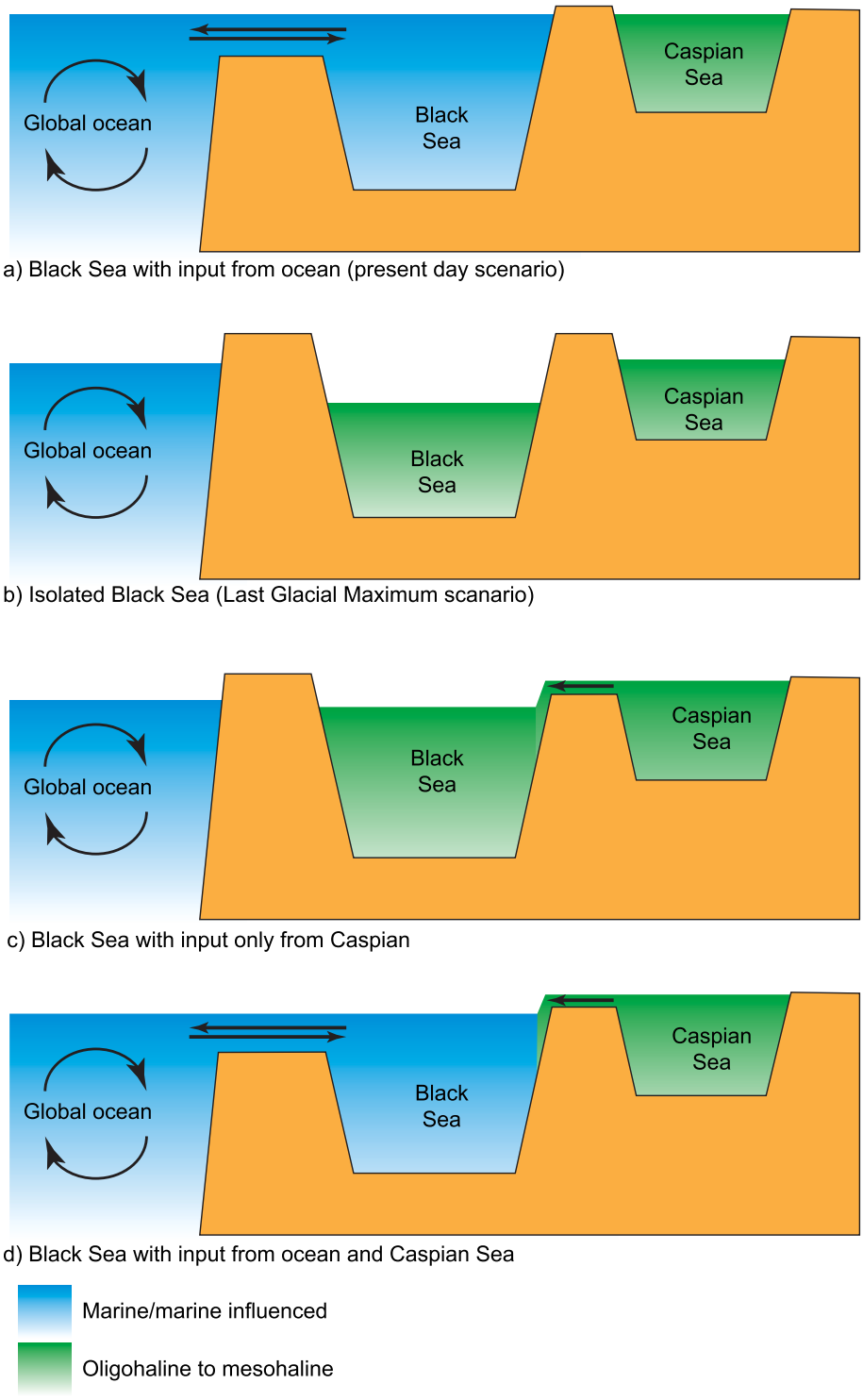

Fig. 2. Schematic diagrams showing the four connectivity scenarios presented: a) Black Sea with input from the ocean (present day scenario), b) isolated Black Sea (Late Glacial Scenario), c) Black Sea with input only from the Caspian Sea, and dBlack Sea with input from the Caspian Sea and the ocean.

major rivers (Danube, Don and Dnieper) that it is considered negligible in the context of this study.

Mass balance calculations used present day strontium concentrations and $^{87}Sr/^{86}Sr$ for the main Black Sea rivers (Danube, Don and Dnieper), on the assumption that the geology of their respective catchments has not changed significantly in the last 430 kyr. In steady state situations, inflow into the basin is balanced by the outflow. Therefore, the volume conservation equation gives:

$$qBO = qOB + R + P - E \quad (1)$$

where, qOB refers to flux from the open ocean to the Black Sea and qBO refers to the flux from the Black Sea to the open ocean. River discharge, evaporation and precipitation of the Black Sea is given by R, E and P, respectively. Therefore, the Sr concentration and Sr isotopic ratio of the Black Sea can be determined as follows, with subscripts referring to oceanic (O), riverine (R) and Black Sea (B).

Sr concentration:

Table 1
Present day fluxes, Sr concentration and Sr isotopic ratio of various water sources into the Black Sea.

Input sources	Fluxes (m^3/yr)	Sr conc. (ppm)	$^{87}Sr/^{86}Sr$
Open ocean	2×10^{11} (Esin et al., 2010)	7.85 (Veizer, 1989)	0.709161–0.709175 (McArthur et al., 2012, LOWESS V5 data set)
Danube	1.98×10^{11} (Jaoshvili, 2002)	0.24 (Palmer and Edmond, 1989)	0.7089 (Palmer and Edmond, 1989)
Don	2.94×10^{10} (Jaoshvili, 2002)	0.22 (Palmer and Edmond, 1989)	0.70840 (Palmer and Edmond, 1989)
Dnieper	4.3×10^{10} (Jaoshvili, 2002)	0.22 (Palmer and Edmond, 1989)	0.70840 (Palmer and Edmond, 1989)
Caspian Sea	Not known	9.92 (Clauer, 2000)	0.708183 (Clauer, 2000)
Present Day (Black Sea + Open Ocean)			0.709133 ± 0.000015 (Major et al., 2006- Supp. Info) 0.709159 (eq. 3)
Isolated Black Sea			0.70874 ± 0.00008 (LGM; Major et al., 2006) 0.708775 (eq. 3)

$$[Sr]_B = ([Sr]_O \times qOB + [Sr]_R \times R)/(qOB + R) \quad (2)$$

and Sr isotopic ratio:

$$^{87}Sr/^{86}Sr_B = \{^{87}Sr/^{86}Sr_O \times [Sr]_O \times qOB + {}^{87}Sr/^{86}Sr_R \times [Sr]_R \times R\}/\{[Sr]_O \times qOB + [Sr]_R \times R\} \quad (3)$$

Input from the Caspian Sea, which has a present day value of 0.708183 (Clauer, 2000), will decrease the Black Sea $^{87}Sr/^{86}Sr$ below its isolated value but this is not calculated here due to lack of constraint on past Caspian Sea influx rates.

3. Results

3.1. Palynology

Dinocysts are abundant in all samples analysed (Fig. 3) except for one sample, at 272 mbsf, which was barren. All palynological and strontium data are provided in supplementary information. Most of the studied interval consists of high relative abundances of the dinocyst *Pyxidinopsis psilata* sensu stricto (Fig. 3). However, many dinocyst morphotypes fall on a gradient between described endmember taxa, as described by Hoyle et al. (2019). Codes used here for undescribed forms relate to the figure number and plate letter of the dinocyst variability matrix of Hoyle et al. (2019). *Pyxidinopsis psilata* ranges from psilate, round to cruciform as originally described by Wall and Dale (1973) to the rugose forms described by Marret et al. (2004), to morphotypes displaying traces of paratabulation (faint sutures as well as incipient processes) as described by Head et al. (1993). In the current study these have been split into *P. psilata* sensu stricto (Fig. 3 a of Hoyle et al., 2019) and *P. psilata* var. A (3b) of Hoyle et al. (2019). We include all *Pyxidinopsis psilata* specimens lacking traces of paratabulation in *Pyxidinopsis psilata* sensu stricto (Fig. 3 a, e, i and m of Hoyle et al., 2019). Dinocyst A (Fig. 1 k-l), dinocyst B (Fig. 1j), dinocyst C (Fig. 3 c), dinocyst sp. D (Fig. 3 d), and dinocyst F (Fig. 1 q-r) (Hoyle et al., 2019) were also encountered in the studied sequence. Species described from the Late Glacial of the Black Sea were also encountered, including *Spiniferites cruciformis* and *Impagidinium inaequalis* (Wall et al., 1973; Wall and Dale, 1973).

Dinocysts of Paratethyan lineage, indicating oligohaline to mesohaline environments, were encountered, including *Caspidinium rugosum*, *Impagidinium spongianum*, *Komewuia*? sp. (Baltes, 1971; Marret et al., 2004; Mudie et al., 2017; Rundić et al., 2011; Soliman and Riding, 2017) mainly between 100 and 200 mbsf (Fig. 3). Other forms encountered (*Impagidinium* var. cruciform, Dinocyst F, Hoyle et al., 2019) have not previously been described, and therefore only limited (if any) ecological inference can be made based on their occurrence at present, even if they are abundant in some levels (e.g. Dinocyst F, 47% at 174.31 m).

Between ~175 and 120 mbsf, *Caspidinium rugosum*, *Impagidinium inaequalis*, *Impagidinium spongianum* and heterotrophic cysts are at their most common. *Impagidinium* var. cruciform appears at the base of this interval and becomes more common towards the top, reaching its acme at 120.41 mbsf before dropping off to low percentages again. *Spiniferites cruciformis* is common between 275 and 255 mbsf (with trace occurrences of *Impagidinium* var. cruciform).

Peaks of *Lingulodinium machaerophorum* with processes (diagnostic spine-like protuberances on the outside of the cyst) > 10 μm occur at 95.72 mbsf (37%) and 229.91 mbsf (74%). It has been observed that *Lingulodinium machaerophorum* grows shorter processes in low salinity environments (Mertens et al., 2009). *Operculodinium centrocarpum* sensu Wall and Dale (1966) and *Tectatodinium pellitum*? also occur (mostly at 95.72 mbsf). These taxa are representative of mesohaline to euhaline environments (Zonneveld et al., 2013).

Pollen is abundant throughout the record, and counts of ~300 grains were reached in all samples (Fig. 3 and Suppl. Info). The pollen signal shows variation in relative abundances of different vegetation types with *Pinus* more abundant at the bottom of the record (~275–240 mbsf), while deciduous forest vegetation (*Betula*, *Fraxinus*, *Engelhardia*, *Juglans*, *Carya*, *Pterocarya*, *Acer*, *Tilia*, *Ulmus-Zelkova*, *Carpinus*, *Quercus*, *Alnus*, *Fagus*, *Castanea*, *Nyssa*, *Salix*, *Myrica* and *Corylus*) showed a prominent peak at ~96 mbsf, with noteworthy increases (> 20%) also occurring at 161 mbsf, 182 mbsf, 230 mbsf and 275 mbsf (Fig. 3). Typical arid environment, xerophytic taxa (*Ephedra*, Amaranthaceae, Caryophyllaceae, Asteraceae (including *Artemisia* and *Centaurea*), Convolvulaceae, Poaceae, *Calligonum* and *Rhus*) show increase in relative abundance at 196 mbsf, 174 mbsf, 145–104 mbsf and 69–46 mbsf. Highest pollen concentrations (> 10,000/g dry sediment) occurred at 96 mbsf, 161 mbsf, 230 mbsf and 264 mbsf (depths rounded to nearest metre, see Suppl. Info for precise depths).

3.2. Strontium isotopes

Of the 19 samples counted for dinocysts, only 11 contained ostracod material suitable for measuring isotopes (Suppl. Info). The resulting Strontium isotope record all lies below present-day ocean water values (McArthur et al., 2012) with a peak value of 0.70908 at around 100 mbsf and a low value (0.70858) at ~120 mbsf (Fig. 3).

4. Discussion

4.1. Supporting the age model with terrestrial vegetation patterns

The late Miocene to recent age model of the DSDP Leg 42B cores has been published in Van Baak et al. (2016), based on magnetostratigraphy and biostratigraphic tie points linked to the Eemian (MIS 5e)

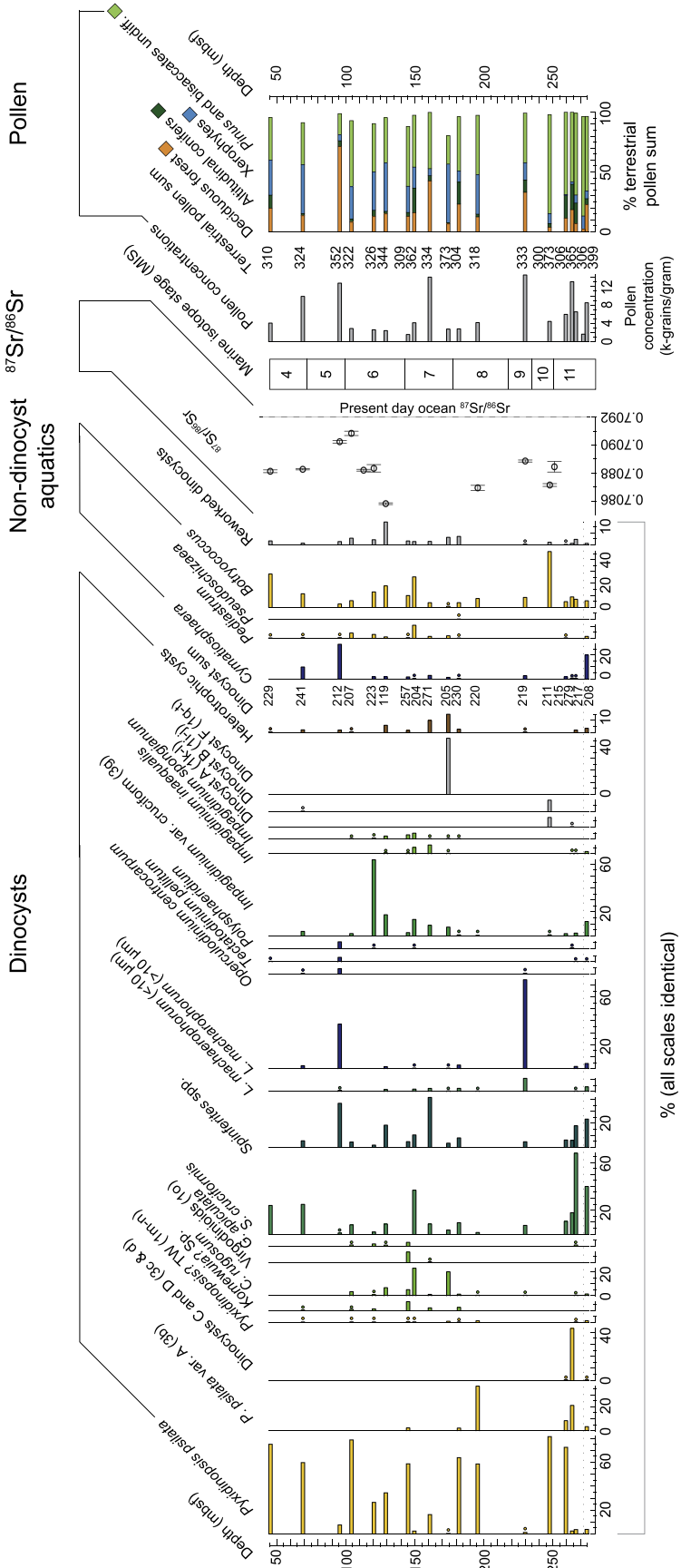

Fig. 3. Diagram showing, from left to right, relative abundances of dinoflagellate cysts, dinocyst sum, dinocyst concentration (thousands of cysts per gram of dry sediment), abundances of selected algae (relative to all aquatic palynomorphs), $^{87}Sr/^{86}Sr$, pollen concentrations (thousands of cysts per gram of dry sediment) and summary pollen diagram showing relative abundance of climate indicative groups. Plotted against depth in metres below sea floor (mbsf) on left axis with non-linear age axis on the right side. Taxa with presence in low percentages are marked on the diagram by a dot. Several of the dinocysts plotted (*Pyxidinopsis psilata* var. A, *Pyxidinopsis*? TW, Virgodinioids and Dinocysts A, B, C, D and F) are defined by Hoyle et al. (2019), and the alphanumeric codes given in parentheses refer to the illustrative plates within that publication.

and Holsteinian (MIS 11) interglacials of Lisiecki and Raymo (2005). Pollen assemblage data independently produced in this study clearly show relatively warm vegetation during interglacial periods (Fig. 3). These assemblages comprise deciduous forest plants, such as *Alnus* (alder), *Carpinus* (hornbeam) and *Fagus* (beech), and higher pollen concentrations suggest an increase in vegetation density during warm periods (Shumilovskikh et al., 2013a). In contrast, pollen of steppe and grassland plants, such as *Artemisia* (wormwood) and Poaceae (grass family), were identified in the glacial intervals, coupled with low overall pollen concentrations, indicating sparser vegetation under glacial climatic regimes.

The pollen data generally show warmer and more humid conditions during the interglacials versus colder and more arid phases, during glacial periods. It is noteworthy that the relatively warm/humid pollen assemblage (that is likely to correspond to MIS11) shows a sudden and short increase, suggesting that there may be a hiatus or an interval of low sediment accumulation at the base of the sequence. However, this may be difficult to test due to the presence of core gaps in that part of the record (Shipboard Scientific Staff, 1978). It is also clear that increased resolution of the palynological record would allow correlation with the global palaeoclimatic framework to be made with a greater degree of certainty.

4.2. Glacial intervals: MIS 4, 6, 8 and 10

During the intervals provisionally interpreted as glacial periods *Pyxidinopsis psilata* sensu stricto (e.g. Fig. 3a of Hoyle et al. (2019) and Figs. 3 and 4) dominates the dinocyst assemblage. This dinocyst is not prevalent during much of MIS 6 but is still more than five times more abundant than in the Black Sea today (Mudie et al., 2017). This is likely to indicate oligohaline to lower mesohaline salinities (between approximately 3 and 10 psu (Brenner, 2001; Wall and Dale, 1973)), and is consistent with the Black Sea being isolated from the Mediterranean during periods of low eustatic sea-level (Grant et al., 2014). The $^{87}Sr/^{86}Sr$ of the Black Sea with no exchange or input from the Mediterranean can be calculated assuming present day river fluxes and gives a Sr isotope ratio of 0.708775 (Table 1) (Eq. 3). Although the dinocyst assemblages are analogous with those in coastal areas of the present day Baltic Sea (which is connected to the ocean via restricted gateways), strontium isotope ratios for samples from all four probable glacial periods lie close to (or below) this calculated value for an isolated Black Sea, supporting the case for complete separation from the Mediterranean at these times.

4.3. Interglacials of MIS 5 and 9

Influxes and dominance of dinocyst species indicating increased salinities in the surface waters occur during MIS 5 and MIS 9 (saline indicators in Fig. 4). In particular, the dominance or high abundance of *Lingulodinium machaerophorum* with well-developed processes (> 10 μm) indicates relatively saline conditions when encountered in the modern Pontocaspian region (~16–18 psu) and suggests that the water column was stratified, at least seasonally (Mudie et al., 2017). *Lingulodinium machaerophorum* can occur at lower salinities (~13 psu in the modern Caspian Sea), but tends to show reduced process length. The long process form, which is the dominant form observed during the current study, does not generally dominate assemblages in salinities below ~16 psu (Mertens et al., 2012; Mudie et al., 2017).

The MIS 5 interval also contains dinocysts that are unambiguously characteristic of marine influenced systems, e.g. *Spiniferites ramosus* s.l. and *S. mirabilis* s.l. (Rochon et al., 1999), as well as *Operculodinium centrocarpum* sensu Wall and Dale (1966), *Tectatodinium pellitum*, *Pentapharsodinium dalei*, *Nematosphaeropsis labyrinthus* and *Polysphaeridium zoharyi*. High abundances of *Pterosperma* (*Cymatiosphaera*) are also observed in the MIS 5 interval in this study, which has been used as a tracer of marine input in studies of MIS 5 from other Black Sea cores (Shumilovskikh et al., 2013b). Samples from the MIS 9 interval are dominated by *Lingulodinium machaerophorum* (processes > 10 μm), with rare *Operculodinium centrocarpum* sensu Wall and Dale (1966) (saline indicators in Fig. 4).

The Black Sea's Sr isotope ratio today is dominated by input from the Mediterranean (Major et al., 2006), giving it a ratio that is within error of the global ocean value (McArthur et al., 2012). The two MIS 5 samples have $^{87}Sr/^{86}Sr$ that are the closest to modern values within the entire sampled sequence, approaching present day Black Sea ratios (Fig. 4). Combined with the dinocyst assemblage indications of Black Sea salinities in excess of ~16 psu (Mudie et al., 2017), which are also close to present day values of ~17 psu, these data are broadly consistent with a Black Sea - Mediterranean connection during MIS 5. Exchange between the two basins is likely to have been the result of high interglacial sea-level (Shackleton et al., 2003). At the MIS 6 – MIS 5 transition, the shift towards higher $^{87}Sr/^{86}Sr$ values precedes the peak isotope value of the MIS 5 interglacial and the change in dinocyst assemblages (Fig. 4). Notably, the oxygen isotopes from the Solfular cave are missing and/or show negative values and the relative sea-level reconstructions display low values (Badertscher et al., 2011), but with a large error margin. It is therefore difficult to explain such relatively high values in the $^{87}Sr/^{86}Sr$, unless we assume that the chemistry of the water changed several thousands of years before the biota in the surface waters responded. Although no practicable means of improving the age control is currently available, it is worth noting that Wegwerth et al. (2014) observed similarly high Sr isotopic ratios measured on ostracods collected from a south east Black Sea core between 134 and 130 ka. These authors attributed the phenomenon to pulses of meltwater entering the Black Sea (BSWP II2) at the termination of MIS 6 (Wegwerth et al., 2014). It is possible, therefore, that the peak in Sr ratio along with the low-salinity dinocyst assemblages could indicate change in source water into the Black Sea at ~136 ka, prior to the marine connection. This data point, along with the source of meltwater, will be discussed in detail in Bista et al. (in prep).

The $^{87}Sr/^{86}Sr$ of the Black Sea during the interval interpreted as MIS 9 (~320 ka) show values very close to the present-day Danube $^{87}Sr/^{86}Sr$ (Fig. 4). Interpreted independently of biological proxies, this could be explained by an isolated Black Sea with increased input from the Danube. A similar scenario has been suggested for Heinrich event 1, where climatic warming caused disintegration of continental European ice sheets and two major pulses of meltwater into the Black Sea via the Danube catchment, thereby reducing $^{87}Sr/^{86}Sr$ (Major et al., 2006). However, as the dinocyst assemblages suggest that more saline conditions prevailed at this time, some influx of marine water is required. This is especially the case assuming, as is likely, that the current positive hydrologic balance for the Black Sea was already operating (Marzocchi et al., 2016), implying a high (Black Sea) sea-level at a time of high eustatic sea-level. In order to generate a Sr isotope ratio lower than today's Black Sea ratio, the ocean water input must have been substantially smaller than the present-day flux through the Bosporus (2×10^{11} m^3/yr; (Esin et al., 2010 and references therein)). An alternative explanation is that a larger Mediterranean flux was diluted by coeval overspill from the Caspian Sea. However, there is no clear dinocyst evidence for a Black Sea – Caspian Sea connection at this time.

4.4. MIS 6 and 7

Interpretation of the Sr record and dinocyst assemblages for samples from the interval provisionally interpreted to represent MIS 6 and 7 is complex. Both MIS 6 and 7 samples contain Paratethyan dinocysts and the lowest $^{87}Sr/^{86}Sr$ in the record (Fig. 3 and Fig. 4). The lowest ratio is lower than the values calculated for an isolated Black Sea with present day fluvial input (Fig. 4). The Black Sea must therefore have received additional (fresh) water with a low Sr isotope ratio. One possible explanation is that the Black Sea received input from the Caspian Sea, which has a present-day $^{87}Sr/^{86}Sr$ of 0.708183 (Clauer, 2000).

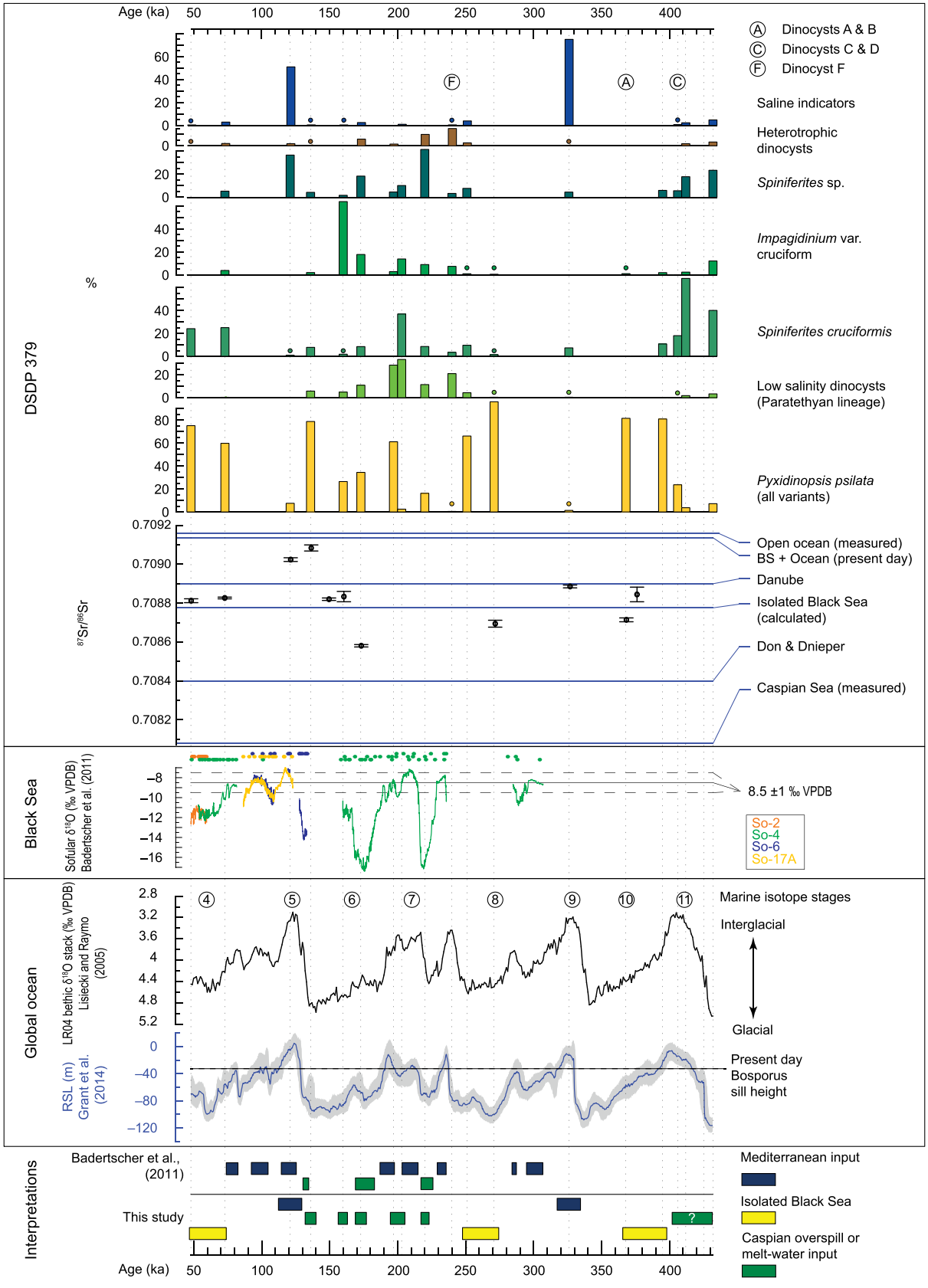

(caption on next page)

Although there are no continuous $^{87}Sr/^{86}Sr$ records of the Caspian Sea over the last 430 kyr, two values measured on *Monodacna* shells from 20 ka (0.70825) and 100 ka (0.70842; Page, 2004), indicate that $^{87}Sr/^{86}Sr$ of the Caspian Sea during this time is likely to have been low. An alternative possibility is that the lowest $^{87}Sr/^{86}Sr$ observed during MIS 6 maybe the result of the enhanced discharge from the Don and/or

Fig. 4. DSDP Site 379 dinocyst and $^{87}Sr/^{86}Sr$ records plotted by age (ka) against data from the wider Black Sea region and from the global ocean. **DSDP 379 box**: cumulative plot showing relative abundances of key dinocyst groups and $^{87}Sr/^{86}Sr$ from DSDP 379. Dinocysts are grouped as follows: Saline indicators = *Lingulodinium machaerophorum* (processes > 10 μm), *Operculodinium centrocarpum* sensu Wall and Dale (1966), *Tectatodinium pellitum*, *Pentapharsodinium dalei*, *Nematophaeropsis labrynthus* and *Polysphaeridium zoharyi*; Heterotrophic cysts = *Lejeunecysta* spp., *Selenopemphix* spp. and *Brigantedinium* spp.; *Spiniferites* spp. = all *Spiniferites* except *S. cruciformis* (does not necessarily indicate marine vs. brackish affinities); *Impagidinium* var. cruciform = affinity unknown; *Spiniferites cruciformis* = all forms; Low salinity dinocysts = *Pyxidinopsis*? var. TW, *Komewuia*? sp. of (Soliman and Riding, 2017), *Caspidinium rugosum*, "Virgodinioid cysts", *Gonyaulax apiculata*, *Impagidinium inaequalis* and *Impagidinium spongianum* (all of which suggest salinities below 13.5 psu); *Pyxidinopsis psilata* = all variants of Hoyle et al. (2019); Letters refer to dinocysts of unknown affinity, as reported by Hoyle et al. (2019). A = dinocysts A & B, C = dinocysts C & D, F = dinocyst F. Presence in low percentages is marked by a dot. **Black Sea box**: stacked Sofular cave $\delta^{18}O$ record of (Badertscher et al., 2011). **Global ocean box:** LR04 benthic $\delta^{18}O$ stack (Lisiecki and Raymo, 2005) and global sea-level curve (Red Sea) of Grant et al. (2014). **Interpretations box:** connection events according to Badertscher et al. (2011) and this study. (For interpretation of the references to colour in this figure legend, the reader is referred to the web version of this article.)

Dnieper rivers.

The presence of *P. psilata* sensu stricto, *S. cruciformis* and the relatively high representation of the freshwater algae *Pediastrum* and *Botryococcus* in the MIS 7 interval suggest that the aquatic environment comprised relatively fresh waters (oligohaline to lower mesohaline). Occasional heterotrophic cysts may indicate good nutrient supply, as their distribution is generally governed by the availability of prey, such as diatoms (Zonneveld et al., 2013). Dinocyst assemblages in what is interpreted as MIS 7 show forms of Paratethyan lineage (e.g. *Impagidinium spongianum* and *Caspidinium rugosum*), as well as a robust form of *Pyxidinopsis* (*Pyxidinopsis*? TW of Hoyle et al., 2019), which is similar to those observed by Soliman and Riding (2017) in sediments from the late Miocene Pannonian Basin. These forms also indicate low salinity conditions. The presence of *Spiniferites* sp. at 220 ka, by contrast cannot be used to determine palaeoenvironmental conditions as these specimens could not be identified to species level, and the genus *Spiniferites* contains both high and low salinity tolerant species (e.g. Richards et al., 2018; Soliman and Riding, 2017; Sütő-Szentai, 2010).

The Paratethyan dinocysts observed in MIS 7 are also present in MIS 6, along with *P. psilata* sensu stricto, again suggesting low salinity conditions. However, the proposed MIS 6 interval also contains *Impagidinium* var. cruciform of Hoyle et al. (2019). The environmental implications of the *Impagidinium* var. cruciform are ambiguous because although it belongs to a genus that generally represents fully marine conditions, its cruciform ambitus is a trait typically associated with low salinities (Wall and Dale, 1973; Zonneveld et al., 2013).

In summary, the dinocyst and algal data suggest that the Black Sea experienced relatively freshwater conditions during both MIS 6 and 7, although ambiguous dating still presents issues for fine scale correlation. Some of the dinocysts are considered to have Paratethyan lineage, suggesting that the lowered salinities could have resulted from a connection with the Caspian Sea. However, as well as occurring in the Caspian Sea (Richards et al., 2018), many of these species also occurred in Black Sea (Grothe et al., 2014) and its satellite basins (e.g. Pannonian Basin) during the Miocene and Pliocene (Baltes, 1971; Soliman and Riding, 2017). An alternative explanation is therefore that these Paratethyan dinocysts were already present in marginal areas, remained in coastal refugia in the Black Sea throughout the Pleistocene and expanded into the open basin only when conditions became favourable e.g. when salinity was lowered due to isolation from the Mediterranean and/or additional fluvial discharge. One further possible implication of the occurrence of these Paratethyan dinocysts is that they reflect a warming of the Black Sea rather than a change in its salinity. This is possible since several of the Paratethyan forms observed (*Caspidinium rugosum*, *Impagidinium spongianum*) have their highest recorded relative abundances during the warm late Miocene (Grothe et al., 2014; Soliman and Riding, 2017).

Interpretation of a connection to the Caspian during MIS 6 and 7 on the basis of the dinocyst assemblage is therefore at best ambiguous and critically there is no unequivocal evidence of Caspian overspill to the Black Sea at this time from other faunal groups (Krijgsman et al., 2019). The hypothesis of lowered Black Sea salinity through additional fluvial discharge is compatible with Badertscher et al. (2011)'s interpretation of the Sofular speleothem (Fig. 4). These authors suggest that increased freshwater discharge due to glacial melt, coupled with reduced evaporation under cold climatic conditions, produced the $\delta^{18}O$ depletion in the cave carbonate record at this time. Given that the Saalian ice sheet covered large parts of the Black Sea catchment during MIS 6 and parts of MIS 7 (Don and Dnieper rivers), this could have generated the additional fluvial discharge required to lower Black Sea salinity. Such a scenario is also compatible with the possible temperature control on some of the Paratethyan dinocysts and the requirement for a mechanism that modifies environmental conditions of the surface waters impacting both the dinocyst assemblages and precipitation that ultimately influences the Sofular record (Fig. 4).

4.5. MIS 11

Near the base of the sequence, potentially equivalent to MIS 11, (with the best age constraint available) the sediment contains an abundance of *Spiniferites cruciformis* and *Spiniferites* spp., with rare occurrences of *Lingulodinium machaerophorum* and *Tectatodinium pellitum,* generally indicative of marine waters. *S. cruciformis* is traditionally associated with "brackish" conditions, occurring today in the Mediterranean, Black Sea, Caspian Sea and Aral Sea (Mudie et al., 2017). However, its range of salinity tolerance is very wide, having been recorded in sediments deposited in fresh water (Lake Kastoria and Lake Sapanca) as well as low percentages in Mediterranean waters with salinities of ~39 psu (Kouli et al., 2001; Leroy and Albay, 2010; Zonneveld et al., 2013).

Occurrence of *P. psilata* var. A (Fig. 3b), Dinocyst C and Dinocyst D (Fig. 3 c-d) of Hoyle et al. (2019) occurs in an apparent transition from *S. cruciformis* dominated assemblages in MIS 11 to *P. psilata* sensu stricto dominated assemblages in MIS 10. This might suggest that these forms could be representative of transitional conditions between upper mesohaline (*S. cruciformis*) and lower mesohaline (*P. psilata* sensu stricto) surface waters (Fig. 3). This is consistent with the idea of environmentally controlled morphological gradients suggested by Hoyle et al. (2019). The signal in the interval interpreted as MIS 11 is therefore difficult to interpret, but is not consistent with strong marine influence. There is no isotope data from this interval as no ostracods were found.

5. Conclusions

Analysis of dinoflagellate cyst assemblages and strontium isotope data from DSDP Site 379 in the central Black Sea indicate substantial changes to surface water environmental conditions and the water sources flowing into the Black Sea during the late Quaternary. During periods potentially related with global sea-level lowstands, glacials MIS 4, MIS 8 and MIS 10, low Sr isotope ratios indicate that the Black Sea was isolated from the Mediterranean. With this source of salt removed, the Black Sea surface water became relatively fresh (3–10 psu), supporting characteristic low-salinity dinoflagellate cyst assemblages.

Both the Sr isotope data and the dinocyst assemblages observed in samples taken from intervals tentatively equated with interglacial periods of MIS 5 and 9 indicate the influence of marine input to the Black Sea. At these times, sea-level rose above the height of the

Bosporus sill, allowing exchange between the two water bodies. The Sr isotope data suggest that during MIS 5, Mediterranean inflow was of similar magnitude to that of the present day (slightly lower) whereas, during MIS 9, the Mediterranean contribution is likely to have been substantially smaller.

The pattern of connection during interglacial highstands and isolation at glacial lowstands is not consistent throughout the record. Dinocyst assemblages from intervals likely related with both glacial MIS 6 and interglacial 7 indicate that the Black Sea freshened during this period. The associated $^{87}Sr/^{86}Sr$ values are very low, suggesting little or no input from the Mediterranean and requiring input either from the Caspian Sea or additional discharge from the Don/Dnieper catchments, perhaps as a result of melting of the Saalian ice sheet. The interpretation of the period likely related to MIS 11 is also unclear as there are no Sr isotope data to test the mesohaline dinocyst assemblages, which suggests Mediterranean input.

Interestingly, each interglacial period documented here possesses a different dinocyst signature and different dinocyst/Sr isotope combinations. If observed in other Black Sea locations, this pattern may provide a useful stratigraphic indicator for characterising and identifying specific late Quaternary interglacial periods. Further work will inevitably be required, including: a) increasing the resolution of the record; b) addressing the difficulties of dating records of palynology and strontium isotope ratios in sedimentary records from the deep basin of the Black Sea, and c) potentially obtaining calcareous benthic foraminifera on which oxygen isotope ratios may be measured for stratigraphic purposes, in order to test the hypotheses presented here.

Declaration of Competing Interest

None

Acknowledgements

This work was part of the PRIDE project, which received funding from the European Union's Horizon 2020 research and innovation programme under the Marie Skłodowska-Curie grant agreement No 642973. Thanks to Holger Kuhlman for facilitating access to the cores and to Sergei Lazarev for help sampling. The authors are grateful to the editor, Prof. Thomas Algeo, and three anonymous reviewers, whose comments contributed to the improvement of the manuscript.

Appendix A. Supplementary data

Supplementary data to this article can be found online at https://doi.org/10.1016/j.palaeo.2020.110069.

References

Albarède, F., Michard, A., 1987. Evidence for slowly changing 87Sr86Sr in runoff from freshwater limestones of southern France. Chem. Geol. 64, 55–65.
Badertscher, S., Fleitmann, D., Cheng, H., Edwards, R.L., Göktürk, O.M., Zumbühl, A., Leuenberger, M., Tüysüz, O., 2011. Pleistocene water intrusions from the Mediterranean and Caspian seas into the Black Sea. Nat. Geosci. 4, 236–239. https://doi.org/10.1038/ngeo1106.
Baltes, N., 1971. Pliocene dinoflagellata and acritarcha in Romania. In: Farinacci, A. (Ed.), Proceedings of the Second Planktonic Conference. Rome, vol. 1970. pp. 1–16.
Bennett, K., 2008. Psimpoll and pscomb. http://chrono.qub.ac.uk/psimpoll/psimpoll.html Software, Queen's University Belfast. Vancouver.
Bennett, C.E., Williams, M., Leng, M.J., Siveter, D.J., Davies, S.J., Sloane, H.J., Wilkinson, I.P., 2011. Diagenesis of fossil ostracods: Implications for stable isotope based palaeoenvironmental reconstruction. Palaeogeogr. Palaeoclimatol. Palaeoecol. 305, 150–161. https://doi.org/10.1016/j.palaeo.2011.02.028.
Birck, J.L., 1986. Precision K-Rb-Sr isotopic analysis: application to Rb-Sr chronology. Chem. Geol. 56, 73–83.
Brand, U., Veizer, J., 1980. Chemical Diagenesis of a Multicomponent Carbonate System-1: Trace elements. J. Sediment. Petrol. 50, 1219–1236.
Brenner, W.W., 2001. Organic-walled microfossils from the Central Baltic Sea, indicators of environmental change and base for ecostratigraphic correlation. Baltica 14, 40–51.
Burke, W.H., Denison, R.E., Hetherington, E.A., Koepnick, R.B., Nelson, H.F., Otto, J.B., 1982. Variation of seawater 87Sr-86Sr throughout Phanerozoic time. Geology 10, 516–519. https://doi.org/10.1130/0091-7613(1982)10<516:VOSSTP>2.0.CO.
Clauer, N., 2000. Fluctuations of Caspian Sea level: beyond climatic variations? Geology 28, 1015–1018.
Cziczer, I., Magyar, I., Pipík, R., Böhme, M., Ćorić, S., Bakrač, K., Sütő-Szentai, M., Lantos, M., Babinszki, E., Müller, P., 2009. Life in the sublittoral zone of long-lived Lake Pannon: Paleontological analysis of the Upper Miocene Szák Formation. Hungary. Int. J. Earth Sci. 98, 1741–1766. https://doi.org/10.1007/s00531-008-0322-3.
De Vernal, A., Marret, F., 2007. Organic-Walled Dinoflagellate Cysts: Tracers of Sea-Surface Conditions. In: Hillaire-Marcel, C., De Vernal, A. (Eds.), Developments in Marine Geology, Proxies in Late Cenozoic Paleoceanography. Elsevier, pp. 371–408. https://doi.org/10.1016/S1572-5480(07)01014-7.
Ellegaard, M., Lewis, J., Harding, I.C., 2002. Cyst-theca relationship, life cycle and effects of temperature and salinity on the cyst morphology of Gonyaulax baltica sp. nov. (Dinophyceae) from the Baltic Sea area. J. Phycol. 38, 775–789.
Esin, N.V., Yanko-Hombach, V., Kukleva, O.N., 2010. Mathematical model of the late Pleistocene and Holocene transgressions of the Black Sea. Quat. Int. 225, 180–190. https://doi.org/10.1016/j.quaint.2009.11.014.
Ferguson, S., Warny, S., Escarguel, G., Mudie, P.J., 2018. MIS 5-1 dinoflagellate cyst analyses and morphometric evaluation of Galeacysta etrusca and Spiniferites cruciformis in southwestern Black Sea. Quat. Int. 465, 117–129. https://doi.org/10.1016/j.quaint.2016.07.035.
Grant, K.M., Rohling, E.J., Bronk Ramsey, C., Cheng, H., Edwards, R.L., Florindo, F., Heslop, D., Marra, F., Roberts, A.P., Tamisiea, M.E., Williams, F., 2014. Sea-level variability over five glacial cycles. Nat. Commun. 5, 5076. https://doi.org/10.1038/ncomms6076.
Grothe, A., Sangiorgi, F., Mulders, Y.R., Vasiliev, I., Reichart, G.J., Brinkhuis, H., Stoica, M., Krijgsman, W., 2014. Black Sea desiccation during the Messinian Salinity Crisis: Fact or fiction? Geology 42, 563–586. https://doi.org/10.1130/G35503.1.
Grothe, A., Andreetto, F., Reichart, G.J., Wolthers, M., van Baak, C.G.C., Vasiliev, I., Stoica, M., Sangiorgi, F., Middelburg, J.J., Davies, G.R., Krijgsman, W., 2020. Paratethys pacing of the Messinian Salinity Crisis: Low salinity waters contributing to gypsum precipitation? Earth Planet. Sci. Lett. 532, 116029. https://doi.org/10.1016/j.epsl.2019.116029.
Head, M.J., Edwards, L.E., Garrett, J.K., Lentin, J.K., Marret, F., Matsuoka, K., Matthiessen, J., O'Mahony, J., Sun, X., De Verteuil, L., Zevenboom, D., 1993. A forum on neogene and quaternary dinoflagellate cysts: the edited transcript of a round table discussion held at the third workshop on Neogene and quaternary dinoflagellates; with taxonomic appendix. Palynology 17, 201–239. https://doi.org/10.1080/01916122.1993.9989428.
Henderson, G.M., Martel, D.J., O'Nions, R.K., Shackleton, N.J., 1994. Evolution of seawater 87Sr/86Sr over the last 400 ka: the absence of glacial/interglacial cycles. Earth Planet. Sci. Lett. 128, 643–651.
Hoyle, T.M., Sala-Pérez, M., Sangiorgi, F., 2019. Where should we draw the lines between dinocyst "species"? Morphological continua in Black Sea dinocysts. J. Micropalaeontol. 38https://doi.org/10.5194/jm-38-55-2019. 55–65.
Ingram, B.L., Sloan, D., 1992. Strontium isotopic composition of estuarine sediments as paleosalinity–paleoclimate indicator. Science (80-.) 255, 68–72.
Jaoshvili, S., 2002. The rivers of the Black Sea. European Environment Agency Technical report 71.
Kouli, K., Brinkhuis, H., Dale, B., 2001. Spiniferites cruciformis: a fresh water dinoflagellate cyst? Rev. Palaeobot. Palynol. 113, 273–286. https://doi.org/10.1016/S0034-6667(00)00064-6.
Krijgsman, W., Stoica, M., Hoyle, T.M., Jorissen, E.L., Lazarev, S., Rausch, L., Bista, D., Alçiçek, M.C., Ilgar, A., van den Hoek Ostende, L., Mayda, S., Raffi, I., Flecker, R., Mandic, O., Neubauer, T.A., Wesselingh, F.P., 2020. The myth of the Messinian Dardanelles: Late Miocene stratigraphy and palaeogeography of the ancient Aegean-Black Sea gateway. Palaeogeography, Palaeoclimatology, Palaeoecology 560, 1–22. https://doi.org/10.1016/j.palaeo.2020.110033. 110033.
Krijgsman, W., Tesakov, A., Yanina, T., Lazarev, S., Danukalova, G., Van Baak, C.G.C., Agustí, J., Alçiçek, M.C., Aliyeva, E., Bista, D., Bruch, A.A., Büyükmeriç, Y., Bukhsianidze, M., Flecker, R., Frolov, P., Hoyle, T.M., Jorissen, E.L., Kirscher, U., Koriche, S.A., Kroonenberg, S.B., Lordkipanidze, D., Oms, O., Rausch, L., Singarayer, J., Stoica, M., Van de Velde, S., Titov, V.V., Wesselingh, F.P., 2019. Quaternary time scales for the Pontocaspian domain: interbasinal connectivity and faunal evolution. Earth-Sci. Rev. 188, 1–40. https://doi.org/10.1016/j.earscirev.2018.10.013.
Leroy, S.A.G., Albay, M., 2010. Palynomorphs of brackish and marine species in cores from the freshwater Lake Sapanca, NW Turkey. Rev. Palaeobot. Palynol. 160, 181–188. https://doi.org/10.1016/j.revpalbo.2010.02.011.
Lewis, J., Taylor, J.D., Neale, K., Leroy, S.A.G., 2018. Expanding known dinoflagellate distributions: investigations of slurry cultures from Caspian Sea sediment. Bot. Mar. 61, 21–31.
Lisiecki, L.E., Raymo, M.E., 2005. A Pliocene-Pleistocene stack of 57 globally distributed benthic δ18O records. Paleoceanography 20, 1–17. https://doi.org/10.1029/2004PA001071.
Major, C.O., Goldstein, S.L., Ryan, W.B.F., Lericolais, G., Piotrowski, A.M., Hajdas, I., 2006. The Co-Evolution of Black Sea Level and Composition through the Last Deglaciation and its Paleoclimatic Significance 25, 2031–2047. https://doi.org/10.1016/j.quascirev.2006.01.032.
Marret, F., Bradley, L., De Vernal, A., Hardy, W., Kim, S-Y., Mudie, P., Penaud, A., Pospelova, V., Price, A.M., Radi, T., Rochon, A., 2020. From bi-polar to regional distribution of modern dinoflagellate cysts, an overview of their biogeography. Marine Micropaleontology 159, 1–15. https://doi.org/10.1016/j.marmicro.2019.101753. 101753.
Marret, F., Leroy, S.A.G., Chalié, F., Gasse, F., 2004. New organic-walled dinoflagellate cysts from recent sediments of Central Asian seas. Rev. Palaeobot. Palynol. 129, 1–20.

https://doi.org/10.1016/j.revpalbo.2003.10.002.
Marzocchi, A., Flecker, R., Van Baak, C.G.C., Lunt, D.J., Krijgsman, W., 2016. Mediterranean outflow pump: an alternative mechanism for the Lago-mare and the end of the Messinian Salinity Crisis. Geology 44, 523–526. https://doi.org/10.1130/G37646.1.
McArthur, J.M., Howarth, R.J., Shields, G.A., 2012. Strontium Isotope Stratigraphy. In: Gradsteini, F.M., Ogg, J.G., Schmitz, M., Ogg, G. (Eds.), The Geologic Timescale. Elsevier, Oxford, pp. 127–144. https://doi.org/10.1016/B978-0-444-59425-9.00007-X.
Menke, B., 1976. Pliozäne und ältestquartäre Sporen- und Pollenflora von Schleswig-Holstein. Geol. Jahrb. R. A 32, 0–196.
Mertens, K.N., Ribeiro, S., Bouimetarhan, I., Caner, H., Combourieu-Nebout, N., Dale, B., De Vernal, A., Ellegaard, M., Filipova-Marinova, M.V., Godhe, A., Goubert, E., Grøsfjeld, K., Holzwarth, U., Kotthoff, U., Leroy, S.A.G., Londeix, L., Marret, F., Matsuoka, K., Mudie, P.J., Naudts, L., Peña-Manjarrez, J.L., Persson, A., Popescu, S., Pospelova, V., Sangiorgi, F., Van der Meer, M.T.J., Vink, A., Zonneveld, K.A.F., Vercauteren, D., Vlassenbroeck, J., Louwye, S., 2009. Process length variation in cysts of a dinoflagellate, Lingulodinium machaerophorum, in surface sediments: investigating its potential as salinity proxy. Mar. Micropaleontol. 70, 54–69. https://doi.org/10.1016/j.marmicro.2008.10.004.
Mertens, K.N., Bradley, L.R., Takano, Y., Mudie, P.J., Marret, F., Aksu, A.E., Hiscott, R.N., Verleye, T.J., Mousing, E.A., Smyrnova, L.L., Bagheri, S., Mansor, M., Pospelova, V., Matsuoka, K., 2012. Quantitative estimation of Holocene surface salinity variation in the Black Sea using dinoflagellate cyst process length. Quat. Sci. Rev. 39, 45–59. https://doi.org/10.1016/j.quascirev.2012.01.026.
Moore, P.D., Webb, J.A., 1978. An Illustrated Guide to Pollen Analysis. Hodder and Stoughton, Sevenoaks.
Mudie, P.J., Aksu, A.E., Yasar, D., 2001. Late Quaternary dinoflagellate cysts from the Black, Marmara and Aegean seas: Variations in assemblages, morphology and paleosalinity. Mar. Micropaleontol. 43, 155–178. https://doi.org/10.1016/S0377-8398(01)00006-8.
Mudie, P.J., Rochon, A., Aksu, A.E., Gillespie, H., 2004. Late glacial, Holocene and modern dinoflagellate cyst assemblages in the Aegean-Marmara-Black Sea corridor: Statistical analysis and re-interpretation of the early Holocene Noah's Flood hypothesis. Rev. Palaeobot. Palynol. 128, 143–167. https://doi.org/10.1016/S0034-6667(03)00117-9.
Mudie, P.J., Marret, F., Aksu, A.E., Hiscott, R.N., Gillespie, H., 2007. Palynological evidence for climatic change, anthropogenic activity and outflow of Black Sea water during the late Pleistocene and Holocene: Centennial- to decadal-scale records from the Black and Marmara Seas. Quat. Int. 167–168, 73–90. https://doi.org/10.1016/j.quaint.2006.11.009.
Mudie, P.J., Marret, F., Mertens, K.N., Shumilovskikh, L.S., Leroy, S.A.G., 2017. Atlas of modern dinoflagellate cyst distributions in the Black Sea Corridor: from Aegean to Aral Seas, including Marmara, Black, Azov and Caspian Seas. Mar. Micropaleontol. 134, 1–144. https://doi.org/10.1016/j.marmicro.2017.05.004.
Page, A.G., 2004. Geochemistry and paleoclimate of the Plio-Pleistocene deposits of the Caspian Sea. PhD thesis. Royal Holloway University of London.
Palmer, M.R., Edmond, J.M., 1989. The strontium isotope budget of the modern ocean. Earth Planet. Sci. Lett. 92, 11–26. https://doi.org/10.1016/0012-821X(89)90017-4.
Reille, M., 1992. Pollen et spores d Europe et d Afrique du nord. Laboratoire de Botanique Historique et Palynologie, Marseille.
Reinhardt, E.G., Stanley, D.J., Patterson, R.T., 1998. Strontium paleontological method as a high-resolution paleosalinity tool for lagoonal environments. Geology 26, 1003–1006.
Reinhardt, E.G., Blenkinsop, J., Patterson, R.T., 1999. Assessment of a Sr isotope vital effect (87 Sr / 86 Sr) in marine taxa from Lee Stocking Island. Bahamas 241–246.
Richards, K., Van Baak, C.G.C., Athersuch, J., Hoyle, T.M., Stoica, M., Austin, W.E.N., Cage, A.G., Wonders, A.A.H., Marret, F., Pinnington, C.A., 2018. Palynology and micropalaeontology of the Pliocene - Pleistocene transition in outcrop from the western Caspian Sea , Azerbaijan : Potential links with the Mediterranean , Black Sea and the Arctic Ocean ? Palaeogeogr. Palaeoclimatol. Palaeoecol. 511, 119–143. https://doi.org/10.1016/j.palaeo.2018.07.018.
Rochon, A., de Vernal, A., Turon, J.-L.J.L., Matthiessen, J., Head, M.J., 1999. Distribution of recent dinoflagellate cysts in surface sediments from the North Atlantic Ocean and adjacent seas in relation to sea-surface parameters. Am. Assoc. Stratigr. Palynol. 35, 1–146. https://doi.org/10.1016/0377-8398(94)00016-G.
Rochon, A., Mudie, P.J., Aksu, A.E., Gillespie, H., 2002. *Pterocysta* gen. Nov.: a new dinoflagellate cyst from pleistocene glacial-stage sediments of the black and Marmara Seas. Palynology 26, 95–105. https://doi.org/10.1080/01916122.2002.9989568.
Rundić, L., Ganić, M., Knežević, S., Soliman, A., 2011. Upper Miocene Pannonian sediments from Belgrade (Serbia): new evidence and paleoenvironmental considerations. Geol. Carpath. 62. https://doi.org/10.2478/v10096-011-0021-z.
Schrader, H.-J., 1978. 41. Quaternary through Neogene history of the Black Sea, deduced from the paleoecology of diatoms, silicoflagellates, ebridians, and chrysomonads. Initial reports Deep Sea Drill. Proj. Vol. 42. Part 2, 789–901.
Shackleton, N.J., Sánchez-Goñi, M.F., Pailler, D., Lancelot, Y., 2003. Marine isotope substage 5e and the Eemian interglacial. Glob. Planet. Chang. 36, 151–155. https://doi.org/10.1016/S0921-8181(02)00181-9.
Shipboard Scientific Staff, 1978. 3. Site 379. In: Ross, D.A., Neprochnov, Y.P. (Eds.), Initial Reports of the Deep Sea Drilling Project, Volume 42, Part 2. U.S. Government Printing Office, Washington, pp. 29–118.
Shumilovskikh, L.S., Arz, H.W., Wegwerth, A., Fleitmann, D., Marret, F., Nowaczyk, N., Tarasov, P.E., Behling, H., 2013a. Vegetation and environmental changes in Northern Anatolia between 134 and 119ka recorded in Black Sea sediments. Quat. Res. (United States) 80, 349–360. https://doi.org/10.1016/j.yqres.2013.07.005.
Shumilovskikh, L.S., Marret, F., Fleitmann, D., Arz, H.W., Nowaczyk, N., Behling, H., 2013b. Eemian and Holocene Sea-surface conditions in the southern Black Sea: Organic-walled dinoflagellate cyst record from core 22-GC3. Mar. Micropaleontol. 101, 146–160. https://doi.org/10.1016/j.marmicro.2013.02.001.
Soliman, A., Riding, J.B., 2017. Late Miocene (Tortonian) gonyaulacacean dinoflagellate cysts from the Vienna Basin. Austria. Rev. Palaeobot. Palynol. 244, 325–346. https://doi.org/10.1016/j.revpalbo.2017.02.003.
Sütő-Szentai, M., 2010. Definition and description of new dinoflagellate genus, species and subspecies from the Pannonian Stage (Hungary). Acta Nat. Pannonica 1, 223–239.
Svitoch, A.A., Selivanov, A.O., Yanina, T.A., 2000. Paleohydrology of the Black Sea Pleistocene Basins. Water Res. 27, 655–664. https://doi.org/10.1023/A:1026661801941.
Van Baak, C.G.C., Vasiliev, I., Palcu, D.V., Dekkers, M.J., Krijgsman, W., 2016. A Greigite-based Magnetostratigraphic Time Frame for the late Miocene to recent DSDP Leg 42B Cores from the Black Sea. Front. Earth Sci. 4, 1–18. https://doi.org/10.3389/feart.2016.00060.
Vasiliev, I., Reichart, G.J., Davies, G.R., Krijgsman, W., Stoica, M., 2010. Strontium isotope ratios of the Eastern Paratethys during the Mio-Pliocene transition; Implications for interbasinal connectivity. Earth Planet. Sci. Lett. 292, 123–131. https://doi.org/10.1016/j.epsl.2010.01.027.
Veizer, J., 1989. Strontium isotopes in seawater through time. Annu. Rev. Earth Planet. Sci. 17, 141–167.
Wall, D., Dale, B., 1966. "Living Fossils" in Western Atlantic Plankton. Nature 211, 1025–1026.
Wall, D., Dale, B., 1973. Paleosalinity relationships of dinoflagellates in the late quaternary of the black sea—a summary. Geosci. Man 7, 95–102. https://doi.org/10.1080/00721395.1973.9989739.
Wall, D., Dale, B., Harada, K., 1973. Descriptions of new fossil dinoflagellates from the late Quaternary of the Black Sea. Micropaleontology 19, 18–31.
Wegwerth, A., Dellwig, O., Kaiser, J., Ménot, G., Bard, E., Shumilovskikh, L., Schnetger, B., Kleinhanns, I.C., Wille, M., Arz, H.W., 2014. Meltwater events and the Mediterranean reconnection at the Saalian–Eemian transition in the Black Sea. Earth and Planetary Science Letters 404, 124–135. https://doi.org/10.1016/j.epsl.2014.07.030.
Yanina, T.A., 2012. Correlation of the late Pleistocene paleogeographical events of the Caspian Sea and Russian Plain. Quat. Int. 271, 120–129. https://doi.org/10.1016/j.quaint.2012.06.003.
Yanina, T.A., Sorokin, V., Bezrodnykh, Y., Romanyuk, B., 2017. Late Pleistocene climatic events re fl ected in the Caspian Sea geological history (based on drilling data). Quat. Int. 1–12. https://doi.org/10.1016/j.quaint.2017.08.003.
Zonneveld, K.A.F., Marret, F., Verreussel, R., Bogus, K., Bonnet, S., Bouimetarhan, I., Crouch, E., De Vernal, A., Elshanawany, R., Edwards, L., Esper, O., Forke, S., Grøsfjeld, K., Henry, M., Holzwarth, U., Kielt, J.F., Kim, S., Ladouceur, S., Ledu, D., Chen, L., Limoges, A., Londeix, L., Lu, S.H., Mahmoud, M.S., Marino, G., Matsuoka, K., Matthiessen, J., Mildenhal, D.C., Mudie, P.J., Neil, H.L., Pospelova, V., Qi, Y., Radi, T., Richerol, T., Rochon, A., Sangiorgi, F., Solignac, S., Turon, J.L., Verleye, T.J., Wang, Y., Wang, Z., Young, M.D., 2013. Atlas of modern dinoflagellate cyst distribution based on 2405 data points. Rev. Palaeobot. Palynol. 191, 1–197. https://doi.org/10.1016/j.revpalbo.2012.08.003.
Zubakov, V.A., 1988. Climatostratigraphic scheme of the Black Sea pleistocene and its correlation with the oxygen-isotope scale and glacial events. Quat. Res. 29, 1–24. https://doi.org/10.1016/0033-5894(88)90067-1.